Aggregation of thrombin-derived C-terminal fragments as a previously undisclosed host defense mechanism

Jitka Petrlova[a,1], Finja C. Hansen[a], Mariena J. A. van der Plas[a], Roland G. Huber[b], Matthias Mörgelin[c], Martin Malmsten[d,e], Peter J. Bond[b,f], and Artur Schmidtchen[a,g,h]

[a]Division of Dermatology and Venereology, Department of Clinical Sciences, Lund University, SE-221 84 Lund, Sweden; [b]Bioinformatics Institute (A*STAR), 138671 Singapore; [c]Division of Infection Medicine, Department of Clinical Sciences, Lund University, SE-221 84 Lund, Sweden; [d]Department of Pharmacy, Uppsala University, SE-75123 Uppsala, Sweden; [e]Department of Pharmacy, University of Copenhagen, DK-2100 Copenhagen, Denmark; [f]Department of Biological Sciences, National University of Singapore, 117543 Singapore; [g]Dermatology, Lee Kong Chian School of Medicine, Nanyang Technological University, 636921 Singapore; and [h]Dermatology, Skane University Hospital, SE-22185 Lund, Sweden

Edited by Barry S. Coller, The Rockefeller University, New York, NY, and approved April 10, 2017 (received for review November 29, 2016)

Effective control of endotoxins and bacteria is crucial for normal wound healing. During injury, the key enzyme thrombin is formed, leading to generation of fibrin. Here, we show that human neutrophil elastase cleaves thrombin, generating 11-kDa thrombin-derived C-terminal peptides (TCPs), which bind to and form amorphous amyloid-like aggregates with both bacterial lipopolysaccharide (LPS) and gram-negative bacteria. In silico molecular modeling using atomic resolution and coarse-grained simulations corroborates our experimental observations, altogether indicating increased aggregation through LPS-mediated intermolecular contacts between clusters of TCP molecules. Upon bacterial aggregation, recombinantly produced TCPs induce permeabilization of *Escherichia coli* and phagocytic uptake. TCPs of about 11 kDa are present in acute wound fluids as well as in fibrin sloughs from patients with infected wounds. We noted aggregation and colocalization of LPS with TCPs in such fibrin material, which indicates the presence of TCP-LPS aggregates under physiological conditions. Apart from identifying a function of proteolyzed thrombin and its fragments, our findings provide an interesting link between the coagulation system, innate immunity, LPS scavenging, and protein aggregation/amyloid formation.

aggregation | thrombin | lipopolysaccharides | host defense peptides

Skin wounds pose a potential threat for invasive infection and sepsis. It is therefore not surprising that multiple host defense systems have developed over the course of evolution that involve initial hemostasis, fibrin formation, and the subsequent action of multiple proteins and peptides of our innate immune system (1–3). In humans, such host defense systems include neutrophil-derived α-defensins and the cathelicidin LL-37 (3, 4), but also proteolytic products of plasma proteins, such as heparin cofactor II (5), antithrombin III (6), and thrombin (7–10). Lipopolysaccharide (LPS) sensing by Toll-like receptor 4 is crucial in early responses to infection. However, an excessive LPS response gives rise to dysfunctionality, causing localized inflammation such as is found in infected wounds, but also severe systemic responses such as are seen in sepsis (11). Therefore, clearance and control of endotoxins are critical to maintaining a robust antibacterial response while maintaining control of inflammatory responses. Thrombin-derived C-terminal peptides (TCPs) of roughly 2 kDa [e.g., FYTHVFRLKKWIQKVIDQFGE, HVFRLKKWIQKVIDQFGE (12–14)], which are present in wounds, frequently form helices upon LPS binding and exert antiendotoxic functions in vitro and in vivo (10, 12). From a therapeutic standpoint, a prototypic thrombin-derived peptide, GKY25 (GKYGFYTHVFRLKKWIQKVIDQFGE) has been shown to protect against *Pseudomonas aeruginosa* sepsis, mainly via reduction of both systemic cytokine responses and excessive coagulation (12, 15). Functional and structural studies have thus far focused on this peptide and related low-molecular-weight peptides (10, 12); however, the major 11-kDa TCP form present in wound fluids (10) remains uncharacterized. During the course of our work, we noted that the 11-kDa TCP was notoriously prone to aggregation, which suggests that this structure may present some unique characteristics that differentiate it from smaller TCPs. This finding prompted us to investigate the biological roles of TCPs further.

Results

Purification and Activity of Recombinant TCP. First, we generated a recombinant 96-aa TCP fragment (denoted here as "rTCP$_{96}$") corresponding to the C-terminal fragment cleaved out from thrombin by human neutrophil elastase (HNE) (Fig. S1 *A* and *B*). Circular dichroism (CD) spectrometry analysis of rTCP$_{96}$ yielded secondary structure characteristics compatible with the corresponding thrombin region (similar to the B4 peptide). Furthermore, in silico modeling studies showed that an rTCP$_{96}$ structure analogous to the structure of the B4 chain of thrombin adopts a stable fold, with minimal structural drift over extended time scales, comparable to the X-ray structure of γ-thrombin, exhibiting compatible secondary structural content (*Materials and Methods* and Table S1). Purified rTCP$_{96}$ was subjected to heparin-affinity chromatography and was found to elute at a similar salt strength as human γ-thrombin (Fig. S1*C*), compatible with a functional (heparin-binding) activity of rTCP$_{96}$. Consistent with previous findings of endogenous 11-kDa TCP (13), we found that the recombinant form was antimicrobial against *Escherichia coli* in a gel-overlay assay (Fig. S1*D*). The rTCP$_{96}$ also demonstrated antibacterial effects in radial diffusion assays (RDAs)

Significance

The work summarized in this paper is based on the simple but unexpected observation that addition of lipopolysaccharide (LPS) or bacteria to human wound fluids leads to precipitation of protein aggregates, a phenomenon not observed in plasma. Using a broad mix of technologies ranging from biophysical, biochemical, and microbiological methods to fluorescence and electron microscopy, and from in silico modeling to studies on wound materials, we demonstrate here a previously undisclosed role of C-terminal thrombin fragments of about 11 kDa, involving LPS- and bacteria-induced aggregation and scavenging, facilitating clearance and microbial killing. Our findings provide a link between the major coagulation factor thrombin, innate immunity, and amyloid formation.

Author contributions: J.P., M. Malmsten, P.J.B., and A.S. designed research; J.P., F.C.H., M.J.A.v.d.P., and R.G.H. performed research; J.P., F.C.H., M.J.A.v.d.P., R.G.H., M. Mörgelin, M. Malmsten, P.J.B., and A.S. contributed new reagents/analytic tools; J.P., M.J.A.v.d.P., R.G.H., M. Malmsten, P.J.B., and A.S. analyzed data; and J.P. and A.S. wrote the paper.

Conflict of interest statement: A.S. is a founder of in2cure AB, a company developing therapies based on thrombin-derived host defense peptides. The peptide GKY25 and variants are patent-protected.

This article is a PNAS Direct Submission.

Freely available online through the PNAS open access option.

[1]To whom correspondence should be addressed. Email: jitka.petrlova@med.lu.se.

This article contains supporting information online at www.pnas.org/lookup/suppl/doi:10.1073/pnas.1619609114/-/DCSupplemental.

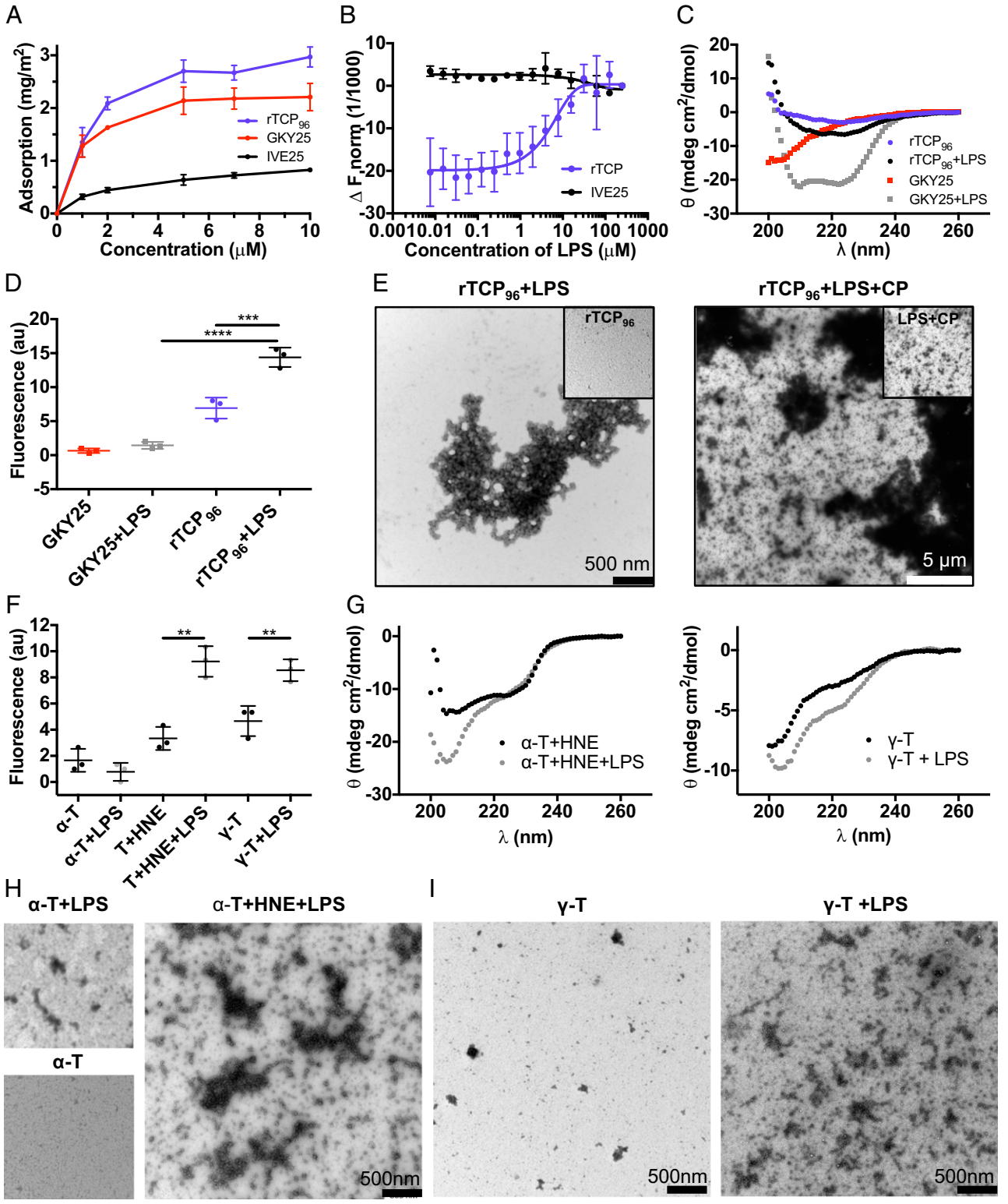

Fig. 1. Analysis of TCP–LPS interactions and LPS-mediated aggregation. (*A*) Ellipsometry analysis revealed adsorption of 1 μM $rTCP_{96}$, GKY25, and IVE25 at LPS-coated surfaces from 10 mM Tris (pH 7.4) (transformation to milligrams of peptide bound per milligram of LPS was achieved by dividing by the amount of LPS preadsorbed: 1.48 ± 0.38 mg/m^2). (*B*) We used an MST assay to quantify the interaction of $rTCP_{96}$ with LPS. The peptide IVE25 was used as a negative control. The mean values of four measurements ± their SDs are shown. (*C*) Changes in the secondary structure of $rTCP_{96}$ triggered by LPS binding were analyzed by CD spectroscopy. The data showed an increase in the β-sheet structure in $rTCP_{96}$ (10 μM) and an increase in the α-helical content in GKY25 (10 μM) after 30 min of incubation with LPS (100 μg/mL) at 37 °C. (*D*) ThT assay, identifying a significant increase in amyloid formation in $rTCP_{96}$ (at 10 μM) after the addition of 100 μg/mL LPS ($n = 3$). au, arbitrary units. ***$P < 0.001$, ****$P < 0.0001$. (*E*) Negative-stain TEM revealed the formation of aggregates after incubation of $rTCP_{96}$ with LPS in 10 mM Tris (pH 7.4) and supplemented with citrated plasma (CP). (*Insets*) Same samples without LPS treatment using the same magnification. Structural changes in digested α-thrombin (α-T; 10 μM) by HNE and γ-thrombin (γ-T) were recorded via ThT assay (*F*) and CD spectroscopy (*G*). Thrombin was used as a control. (*H* and *I*) TEM analysis of aggregates (1–2 μm in length) present in digested α-T and γ-T (0.1–0.5 μm in length) after incubation with LPS. Only small amounts of aggregates, or none at all, were detected in α-T alone, or after addition of LPS, respectively.

against *E. coli* and *P. aeruginosa* (Fig. S1 *E* and *F*), as well as against *E. coli*, in viable count assays (VCAs), at the concentration range of 0.5–3 μM (Fig. S1 *G* and *H*). The results demonstrate that $rTCP_{96}$, like the native form, and similar to GKY25 comprising the C-terminal 25 aa of $rTCP_{96}$, kills gram-negative bacteria in vitro. Because GKY25 dose-dependently induces hemolysis, we explored whether TCPs could permeabilize human erythrocytes as well, but we did not detect any such effects (Fig. S1*I*).

TCPs Interact with LPS. Based on these findings, we next explored possible LPS–$rTCP_{96}$ interactions and the structural implications of these interactions. Ellipsometry analysis of surface interactions revealed significant binding already at concentrations of 1–2 μM for both $rTCP_{96}$ and GKY25 to surface-immobilized *E. coli* LPS, whereas the negative control IVE25 displayed much lower binding (Fig. 1*A*). As can be seen in Fig. S1*J*, kinetics measurements of LPS binding showed comparable binding kinetics for $rTCP_{96}$ and GKY25, with both displaying an initial mass transport-limited phase for less than ∼200 s, followed by considerably slower binding, most likely as a consequence of structural rearrangements in the LPS layer on peptide binding. Analogously, microscale thermophoresis (MST), a highly sensitive technique probing interactions between components in solution, demonstrated interactions of fluorescence-labeled $rTCP_{96}$ with *E. coli* LPS, with a K_d of 3.3 ± 1.8 μM (Fig. 1*B*). Furthermore, in a slot-blot assay, using biotin-labeled *E. coli* LPS and immobilized $rTCP_{96}$, we observed binding of LPS to $rTCP_{96}$, which was eradicated by the addition of heparin (Fig. S1*K*). Because heparin binds to a region situated at the C terminus of the thrombin molecule, which comprises a part of the exosite II site (16), these results indicate that the C-terminal helical end of $rTCP_{96}$ binds to LPS.

LPS Induces Aggregation of TCPs. The above observations were substantiated using CD spectrometry, and we found that LPS induced a helical conformation in the 25mer thrombin-derived TCP GKY25, consistent with findings of previous studies (10, 17). For comparison, an increase in β-sheet content was observed for $rTCP_{96}$ after 30 min of incubation with LPS (Fig. 1*C*). Thioflavin T (ThT) has become among the most widely used "gold standards" for selectively staining and identifying amyloid fibrils characterized by β-strand–like interactions (18, 19). Unlike the results observed for GKY25 after the addition of LPS, a significant increase in ThT staining was noted after the addition of LPS to $rTCP_{96}$, (Fig. 1*D*), which is consistent with CD data on β-sheet content (Fig. 1*C*). LPS-induced aggregation of TCP_{96} was inhibited by an excess of the peptide GKY25 (Fig. S2*A*). Moreover, LPS-induced ThT binding was observed using a dose range of 1–10 μM $rTCP_{96}$ in Tris buffer and 0.5–10 μM $rTCP_{96}$ in the presence of 1% citrated plasma (Fig. S2*B*). Likewise, LPS induced the formation of amorphous aggregates of $rTCP_{96}$, ranging from 1–3 μm in size, as demonstrated by negative-stain transmission electron microscopy (TEM; Fig. 1*E*). Furthermore, $rTCP_{96}$ was added to a buffer containing citrated plasma. Again, we observed similar LPS-induced aggregation that yielded aggregated forms with sizes ranging from 0.5–30 μm (Fig. 1*E*). Moreover, coaggregation of $rTCP_{96}$ with LPS was confirmed by detection of significant differences in the hydrodynamic radii using dynamic light scattering (DLS; Fig. S2*C*). Using CD spectrometry, a ThT-binding assay, and DLS, we did not detect a significant aggregation of pure $rTCP_{96}$ for a time period up to 2 h, which contrasted to the LPS-induced aggregation observed already after an incubation period of 10 min (Fig. S2 *D–F*).

Although $rTCP_{96}$ mimicked the antibacterial effects of native human TCP, it may be argued that possible differences in folding patterns between the recombinant and endogenous forms could have influenced the observed aggregation of the recombinant peptide. To address this issue, we conducted CD, ThT, and TEM experiments using two fragmented thrombin forms containing TCPs in the form of HNE-digested thrombin or γ-thrombin. The latter is a product of autoproteolysis and contains a TCP that is very similar to the HNE-generated fragment (9, 20). In all cases, the results using these endogenous TCPs were consistent with the results obtained with $rTCP_{96}$, and no significant aggregation was observed for intact thrombin (Fig. 1 *F–I*).

Molecular Simulations of the TCP–LPS Interaction. Next, we performed in silico analyses of the TCP–LPS interaction using both atomic resolution and coarse-grained (CG) molecular dynamics simulations. These simulations allowed us to assess the fold stability of the 11-kDa TCP structure, its conformational changes compared with the conformational changes of intact thrombin, and the interaction modes of LPS with TCP. Our analysis revealed a newly exposed amphipathic helix, comprising residues 80–96, buried within intact thrombin. The hydrophobic portion of this amphipathic helix was observed to interact with a sheet region (residues 46–60); we also found that the hydrophobic portion was in a preferred interaction site for the lipid tails of LPS (Fig. 2*A*). We observed a twist in the β-sheet region in the absence of LPS that enabled the formation of a cluster of hydrophobic residues comprising F52, Y57, M59, F81, W86, and F94 (Fig. 2*A*). Therefore, interactions with LPS may enable relaxation of the sheet twist and, accordingly, may explain the observed increase in β-content in the CD spectra. Coarse-grained models provide a pseudoatomistic description of the system while enabling longer time scales and length scales to be attained, thereby enabling us to study the spontaneous self-assembly of TCP and LPS (Fig. 2*B*, Fig. S3, and Movie S1). These simulations revealed a significantly increased propensity of TCPs to aggregate in the presence of LPS (Fig. 2 *B* and *C*). Pairwise distance analysis (Fig. 2*C*) indeed revealed that the aggregation coincides with the preferred LPS-binding sites on TCP (Fig. 2*A*). Furthermore, inspection of the resultant aggregates revealed that LPS intercalates in the TCP clusters, and thereby facilitates intermolecular interaction (Fig. 2*C*, *Right*). Our in silico results thus correspond elegantly to the experimental data presented above and highlight the unique capabilities of TCPs for structural modulation and specific LPS-mediated intermolecular interactions that enable their aggregation.

TCPs Mediate Bacterial Aggregation and Phagocytosis. Considering that $rTCP_{96}$ and degraded thrombin (10) exert antibacterial effects, we next explored whether $rTCP_{96}$ could form aggregates together with gram-negative (LPS-containing) bacteria. Indeed, incubation of $rTCP_{96}$ with *E. coli* yielded similar amyloid-like ThT-positive amorphous aggregates as previously identified after the addition of LPS (Fig. 3*A*). Using negative-stain TEM, we identified aggregated bacteria and observed signs of membrane perturbations in $rTCP_{96}$-treated cells only (Fig. 3*B*). The impermeable marker FITC was taken up by these bacterial aggregates (Fig. 3*C*), indicative of bacterial killing, which is consistent with the antibacterial effects by $rTCP_{96}$ noted above (Fig. S1 *D–H*). Fig. 3*D* illustrates that although both GKY25 and $rTCP_{96}$ were able to induce uptake of FITC, only $rTCP_{96}$ significantly increased the aggregation of *E. coli* ($P < 0.01$). To explore the functional significance of TCP-mediated aggregation, we hypothesized that aggregate formation was linked to phagocytic clearance. Indeed, we found that fluorescent *E. coli* particles, aggregated with $rTCP_{96}$, were taken up by the macrophage cell line RAW 264.7. Notably, $rTCP_{96}$ at 0.5 μM yielded a roughly 25% increase in phagocytosis compared with *E. coli* particles only ($P < 0.01$; Fig. 3*E*). Phagocytized fluorescent *E. coli* particles (green color), aggregated with $rTCP_{96}$ (visualized using fluorescently labeled antibodies), were also detected in RAW 264.7 cells using fluorescence microscopy (Fig. 3*F* and Fig. S4). Taken together, these results indicate that both the $rTCP_{96}$ and native TCPs are able to aggregate and form amyloid structures, and that this phenomenon is promoted in the presence of LPS or bacteria and followed by phagocytic uptake.

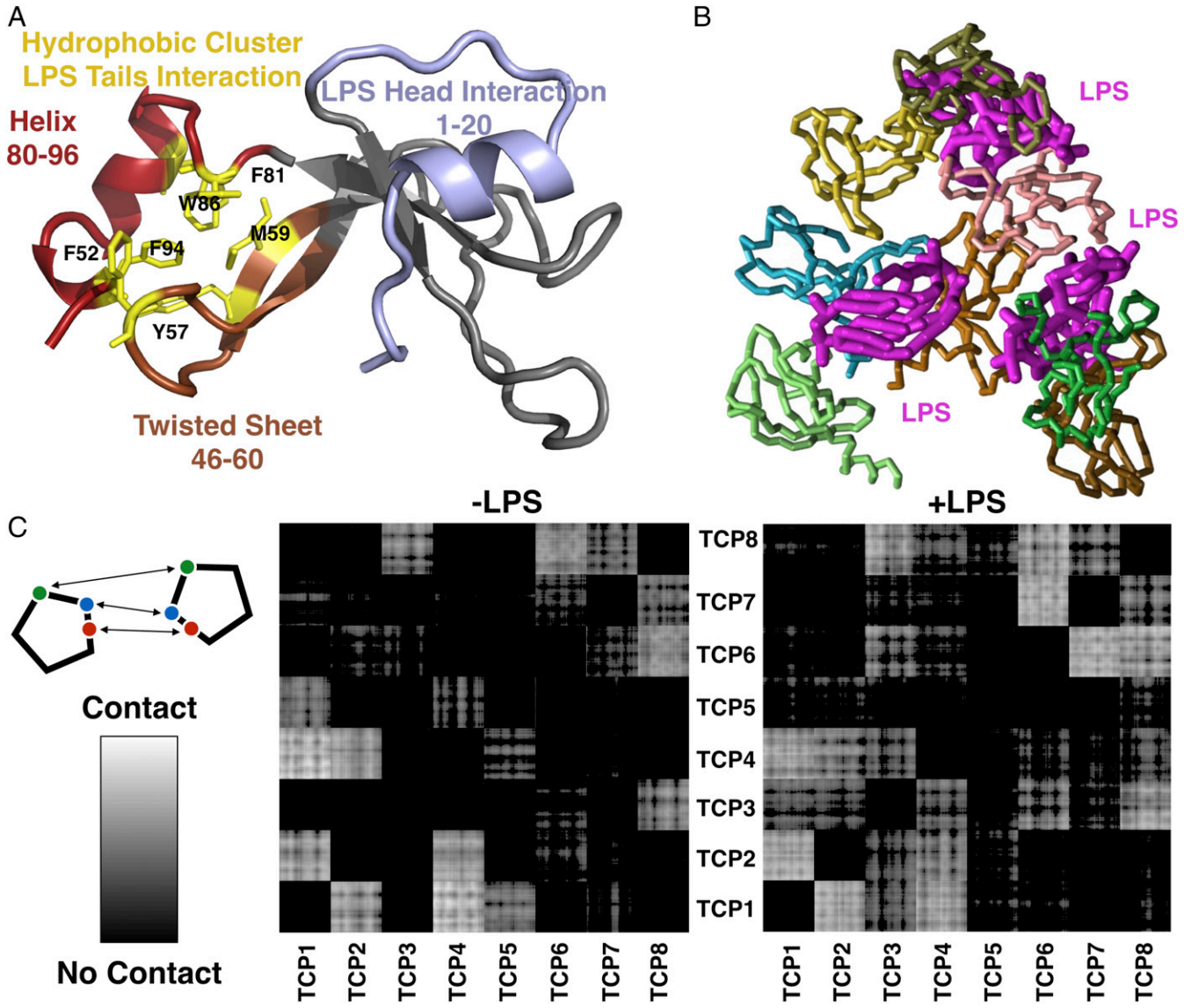

Fig. 2. In silico studies. (*A*) Structure of the 96-aa TCP after 100 ns of atomic resolution molecular dynamics simulations. The hydrophobic residues are shown in gray. The formation of a new hydrophobic cluster (yellow, labeled residues) of the free TCP between the helix segment 80–96 (red) and the sheet residues 46–60 (brown) relies on a twist within the sheet. The extended tail residues formed by residues 46–60 and 80–96 preferentially interact with the lipid tails. The flat patch composed of residues 1–20 (blue) of the 96-aa TCP preferentially interacts with the polar head of LPS. (*B*) Snapshot from a TCP aggregation simulation showing a representative aggregated state that is mediated by LPS molecules (purple, thick lines). The TCP backbones are shown in various colors (thin lines). It is apparent that LPS intercalates within the TCP clusters and predominantly connects the preferential interaction sites. (*C*) Aggregation studies of TCP in the presence (+LPS) and absence (−LPS) of LPS. The panels indicate intermolecular distances of all eight TCP molecules in the simulation box. Bright areas indicate contact with larger bright segments signifying larger contact areas between molecules. Dark areas indicate that the respective molecules do not interact. Increased aggregation is apparent through the appearance of additional bright areas in the system containing LPS.

TCPs Are Present in Wound Fluids and Aggregate with *E. coli* and LPS. Earlier studies have shown that thrombin binds to fibrin clots and that fibrin acts as a reservoir for active thrombin (21). Furthermore, human neutrophils release elastase during the initial phases of wound healing, and the enzyme may cleave thrombin present in the soluble form, as well as when immobilized in fibrin (10). As expected, and compatible with our previous findings, wound fluids from patients with noninfected surgical wounds contained several TCPs (Fig. 4*A*). The concentration of 11-kDa TCPs in wound fluids from patients 1 and 2 was estimated to be 2.7 μM and 0.6 μM, respectively (*Materials and Methods* and Fig. S2*G*). As shown above, $rTCP_{96}$ forms aggregates in a plasma environment (Fig. 1*D*). To address whether endogenous TCPs could also form aggregating amyloid structures, we incubated human wound fluid (from patient 2) with LPS and analyzed aggregate formation. Similar to the in vitro studies described above, we were able to identify LPS-induced aggregates in the wound fluids. By using gold-labeled antibodies, we detected C-terminal epitopes in these structures (Fig. 4*B*). When these experiments were repeated with *E. coli*, we observed a significant aggregation with TEM after the addition of the bacteria to the wound fluid (Fig. 4*C*). These results were supported by confocal microscopy data (Fig. 4 *D* and *E*), where the same initial experimental setup was used, followed by specific staining for TCPs (red) and amyloids (green). Therefore, TCP-containing aggregates were induced after the addition of LPS (Fig. 4*D*) or *E. coli* (Fig. 4*E*), yielding aggregates containing TCPs that overlapped with ThT staining (green), thereby indicating the formation of TCP-containing amyloids. Taken together, these

results demonstrate a proof of principle that TCPs are present in wound fluids at relevant physiological concentrations, where they have the ability to aggregate with *E. coli* and LPS.

TCPs Are Found with Aggregated LPS in Vivo. Nonhealing venous ulcers are characterized by the presence of bacteria accompanied by the activation of neutrophils and the release of HNE (22, 23). We accordingly investigated the production of TCPs in fibrin slough from a patient with such a venous ulcer; we also studied the fluid from a wound dressing covering the ulcer. As shown in Fig. 4*F*, we detected TCPs in both the fibrin and the wound exudate. We next investigated the fibrin slough from nonhealing ulcers from two patients to search for the presence of TCP-LPS aggregates via negative-stain TEM using specific gold-labeled antibodies. The antibodies against TCPs were detected by anti-rabbit IgG with labeled gold particles 10 nm in diameter (blue dots, Fig. 4*G*); for the detection of LPS, we used IgG anti-LPS labeled with 5-nm gold particles (red dots, Fig. 4*G*). A colocalization of TCPs (10-nm particles) and LPS (5-nm particles) was observed in both patient samples, in the range 30–600 nm, with a peak in the lower range (below 50 nm) where the pair cross-correlation function (PCCF) exceeded ∼2 (Fig. S2*H*). Antigens that do not cross-correlate have no PCCF peak in any interval, and the value fluctuates around 1 (24).

Discussion

Endotoxin, a highly proinflammatory substance, as well as bacteria, needs to be contained and controlled, and the present work discloses a simple but effective mechanism by which aggregation-prone TCPs facilitate this clearance, which is of relevance for the control of infection and inflammation during wounding. Apart from revealing a role for thrombin as a source for endotoxin- and bacteria-aggregating peptides during wounding, our results also raise interesting perspectives on the roles of, and relation between, antimicrobial and amyloidogenic peptides. It is clear that various peptides from these two classes are able to bind and damage bacterial and eukaryotic cell membranes. Indeed, it has been proposed that some peptides that are simultaneously antimicrobial and amyloidogenic have separate sequence motifs encoding these two activities (25). Considering the observation that the shorter TCP GKY25 does not form any aggregates, this finding would imply that the sequence responsible for the aggregation behavior, and β-sheet formation, is found upstream of the GKY25 sequence, which is in agreement with in silico predictions. Although structurally separate, our data indicate that the antimicrobial and amyloidogenic properties are interdependent, indeed connecting the antimicrobial and LPS-aggregating functions within one single molecule.

A controlled and targeted proteinase action is crucial during wounding. Thrombin, initially formed by selective proteolysis by coagulation factor X, mediates fibrinogen degradation and clot formation (7) but also exerts other physiological functions in innate defense and hemostasis (7) (Fig. 5). As previously reported, subsequent proteolysis leads to formation of smaller TCPs of about 2 kDa with antiendotoxic functions (10, 14, 15) (Fig. 5). Interestingly, *P. aeruginosa* "hijacks" this mechanism by release of bacterial elastase, which cleaves out a TCP of 21 aa, thereby enabling modulation and circumvention of host responses (14). In many aspects, such TCPs act as "classical" host defense peptides like LL-37 (26), which also binds to LPS, leading to inhibition of NF-κB activation. The herein presented work on LPS and bacteria-induced aggregation of TCPs therefore adds a previously undisclosed dimension to the role of thrombin (Fig. 5). Furthermore, the finding that thrombin fragments, including ∼11-kDa TCPs, are present in acute, sterile wound fluids, together with the rapid aggregation of LPS and bacteria observed in these wounds fluids ex vivo, indicates a fundamental role for aggregation and amyloid formation in the containment and rapid clearance of endotoxins and invading microbes.

This link between host defense and aggregation also suggests that chronic inflammatory states may lead to dysfunctional activation of such host defense pathways. Indeed, amyloidogenic aggregates are implicated in a broad range of protein misfolding diseases, such as Parkinson's disease, Huntington's disease, and Alzheimer's disease (AD). Moreover, amyloidogenic amyloid β-peptide variants have been shown to exert antimicrobial activity (27, 28). Furthermore, peptides derived from the disulfide-constrained loop region of human β-amyloid precursor protein and the N terminus of human prion protein are antimicrobial (29, 30). Interestingly, neutrophils have recently been implicated in the pathogenesis of amyloid deposits in AD of humans as well as in mouse AD models (31), highlighting the importance of peripheral innate immunity for amyloid formation. Thus, hypothetically, because both thrombin and neutrophils are increased in AD (32, 33), high inflammatory activity could lead to degradation of thrombin and generation of amyloidogenic complexes.

In summary, we have revealed here a previously unknown host defense action of proteolyzed thrombin and its fragments, based on LPS-induced aggregation/scavenging, clearance, and microbial killing. Our findings add information to the broad spectra of thrombin functions and provide a link between the coagulation system, host defense, and LPS- and bacteria-induced aggregation and amyloid formation.

Materials and Methods

Ethics Statement. The use of human wound materials was approved by the Ethics Committee at Lund University (LU 708-01 and LU 509-01). Informed consent was obtained from all of the donors, and the use of human blood was approved by the Ethics Committee at Lund University (permit no. 657-2008).

Biological Materials. Fibrin sloughs from chronic nonhealing wounds were collected using a sterile spatula and immediately either fixed in the solution for electron microscopy or frozen at −20 °C for later extraction for SDS/PAGE. Sterile wound fluids were obtained from surgical drainages after surgery. The collection of samples was performed 24 h and 24–48 h after surgery. The wound fluids were centrifuged, aliquoted, and stored at −20 °C.

Microorganisms. The *E. coli* American Type Culture Collection (ATCC) 25922 and *P. aeruginosa* ATCC 27853 bacterial strains were purchased from LGC.

Cells. RAW 264.7 cells (ATCC) were cultured in DMEM (HyClone; GE Healthcare Life Science) supplemented with 10% (vol/vol) heat-inactivated FBS (FBSi; Invitrogen) and 1% (vol/vol) antibiotic/antimycotic solution (AA; Invitrogen).

Peptides. The thrombin-derived peptides GKY25 (GKYGFYTHVFRLKKWIQK VIDQFGE) and IVE25 (IVEGSDAEIGMSPWQVMLFRKSPQE) were synthesized by Biopeptide Co., Inc. We confirmed the purity (over 95%) via mass spectral analysis (Voyager MALDI-TOF; Applied Biosystems).

Digestion of α-Thrombin and Western Blotting. Digestion of α-thrombin (10 μM; Innovative Research, Inc.) was performed for 3 h at 37 °C using 0.8 μg/mL HNE (Calbiochem). The protein and peptides were separated by electrophoresis on a 10–20% tricine gel (Novex; Life Technologies) and subsequently transferred to a PVDF membrane using a Trans-Blot Turbo system (Bio-Rad). Polyclonal rabbit antibodies against the C-terminal thrombin epitope VFR17 (VFRLKKWIQKVIDQFGE; diluted 1:800; Innovagen AB), followed by porcine anti-rabbit HRP-conjugated antibodies (1:1,000; Dako), were used to detect the C-terminal epitopes of thrombin. The TCPs were visualized using chemiluminescent substrates (Thermo Scientific) using a ChemiDoc MP imaging system (Bio-Rad). For quantification of 11-kDa TCPs in wound fluids, $rTCP_{96}$ at concentrations of 0.1, 0.5, 1, and 2 μM (in 2 μL of wound fluid) was analyzed by Western blotting as described above, and used to generate a standard curve using the ChemiDoc MP imaging system and Image Lab software (34). Two microliters of wound fluid from patients 1 and 2 was used for quantification of the 11-kDa fragments present, relative to the standard (illustration is shown in Fig. S2*G*).

Purification of $rTCP_{96}$. A bacterial expression system consisting of pGEX plasmid in *E. coli* strain BL21 codon plus (DE3) RIPL (Invitrogen) was used to produce the $rTCP_{96}$. We cultivated the bacteria in LB (Sigma–Aldrich) supplemented with 34 μg/mL chloramphenicol and 100 μg/mL carbomycin.

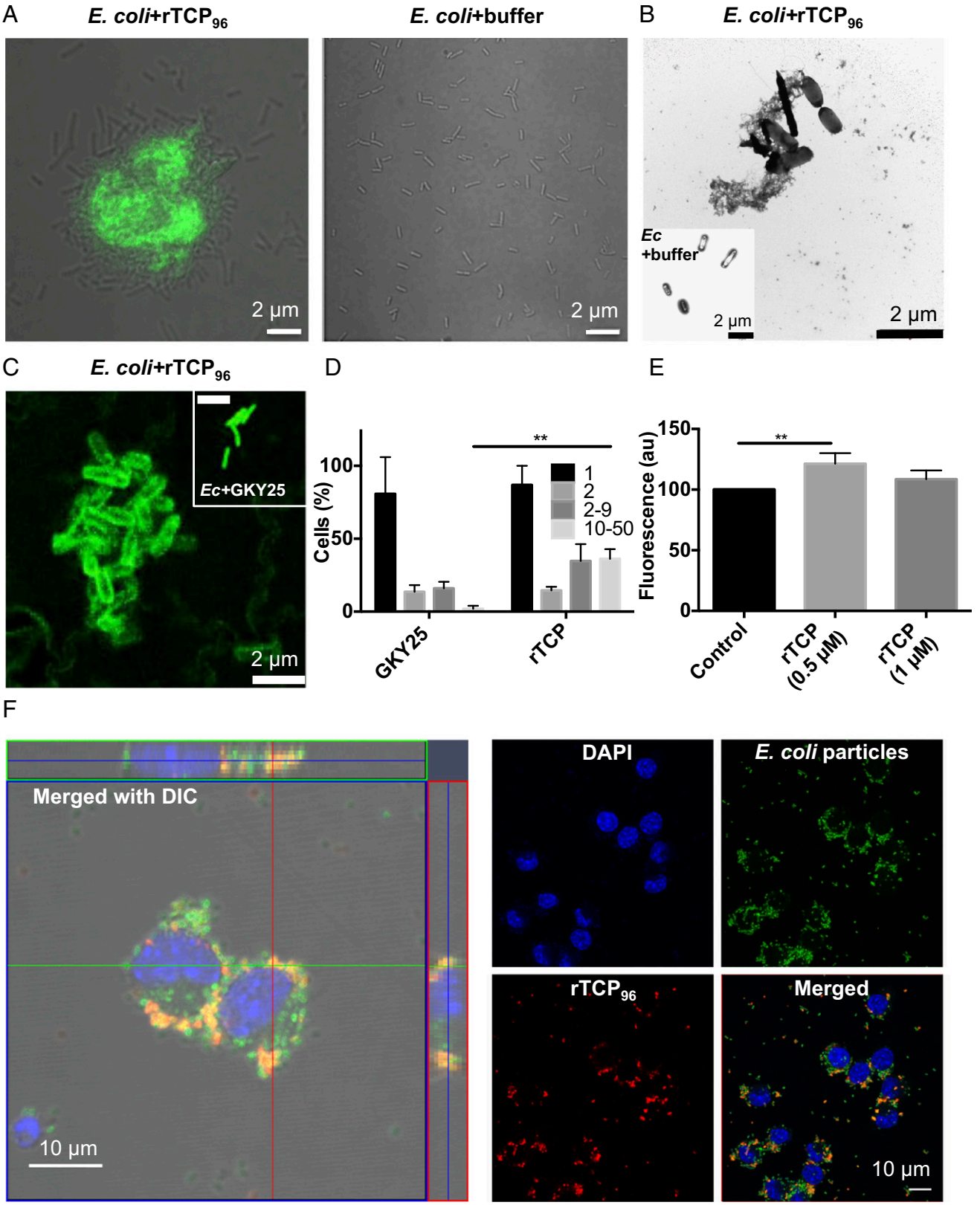

Fig. 3. Coaggregation of *E. coli and* TCPs. (*A*) Confocal microscopy and ThT staining were used to detect *E. coli*-induced amyloid formation of $rTCP_{96}$ (10 μM) in 10 mM Tris buffer (pH 7.4). (*B*) TEM with negative stain analysis reveals the aggregation of $rTCP_{96}$-treated bacteria. (*C*) Fluorescence microscopy shows the agglutination of permeabilized $rTCP_{96}$-treated bacteria after the addition of FITC dye. (*Inset*) GKY25-treated *E. coli* (*Ec*). (*D*) Significant increase in the number of bacteria per aggregate was detected after treatment with 10 μM $rTCP_{96}$ compared with GKY25 ($n = 3$). $^{**}P < 0.01$. (*E*) Phagocytosis assay using the macrophage cell line RAW 264.7 revealed a significant increase in the phagocytosis of *E. coli* particles pretreated with $rTCP_{96}$ (0.5 μM; $n = 4$). $^{**}P < 0.01$. (*F*) Confocal microscopy analysis of phagocytized *E. coli* particles (green) pretreated with $rTCP_{96}$ (Alexa 568, red); we used RAW 264.7 cells (DAPI, blue). DIC, differential interference contrast.

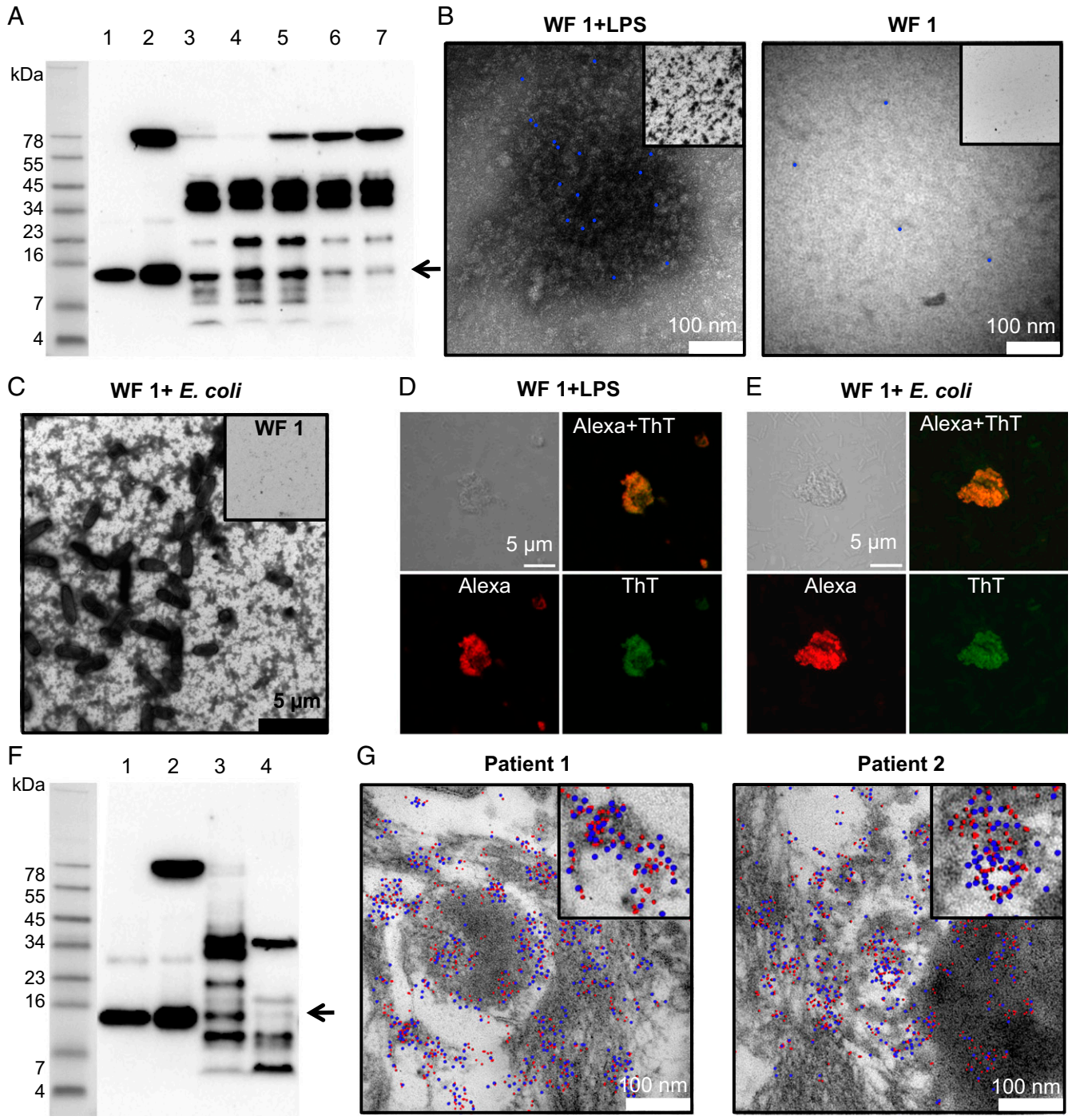

Fig. 4. C-terminal fragments of thrombin are found in human acute wound fluids, fibrin sloughs, and wound dressings. (*A*) Western blotting yielded 11-kDa TCPs in all wound fluid (WF) samples (arrow): (1) $rTCP_{96}$ (10 μM, 1 μL), (2) $rTCP_{96}$ in plasma (10 μM, 1 μL), (3–7) WF from patients 1–5 (patient 1, 80 μg total protein per lane; patients 2–5, 120 μg total protein per lane). (*B*) Ex vivo, aggregates were detected by TEM and demonstrated aggregated endogenous TCPs by using gold-labeled anti-VFR17 epitope IgG (blue dots) in WF after incubation with LPS (*Left*; 100 μg/mL) or without LPS (*Right*). (*Insets*) Display of a 50× lower magnified overview of the same samples. (*C*) Formation of aggregates in WF triggered by *E. coli* bacteria. (*Inset*) WF only, using the same magnification. Confocal microscopy, using primary antibodies against TCPs followed by Alexa 568-labeled secondary antibodies and ThT staining, was used to determine amyloid aggregates containing TCPs in the WF in the presence of LPS (*D*) or *E. coli* (*E*). (*F*) Western blotting of extracts from fibrin slough (FS) and wound dressing revealed the presence of 11-kDa TCP fragments in both samples (arrow): (1) $rTCP_{96}$, (2) $rTCP_{96}$ in CP, (3) extract of FS, and (4) extract of wound dressing. (*G*) Colocalization of endogenous TCPs and LPS in the FS from two patients was detected via TEM analysis. The TCPs were recognized by anti-rabbit IgG with labeled gold particles 10 nm in diameter (blue dots). We detected LPS using IgG against LPS with labeled gold particles 5 nm in diameter (red dots). Colocalization exceeding 90% was observed in both samples. (*Insets*) Same samples using a fourfold higher magnification.

Isopropyl-β-D-thiogalactopyranoside (400 μM; VWR), added at the midlog phase, was used to induce peptide production in the bacterial system. The $rTCP_{96}$ peptides were extracted and purified by immobilized metal affinity chromatography (Ni-NTA Agarose; Invitrogen) under denaturing conditions [8 M urea, 10 mM Tris (pH 7.4)], extensively washed with 20 mM imidazole in 8 M urea and 10 mM Tris (pH 7.4), and then eluted by stepwise increasing

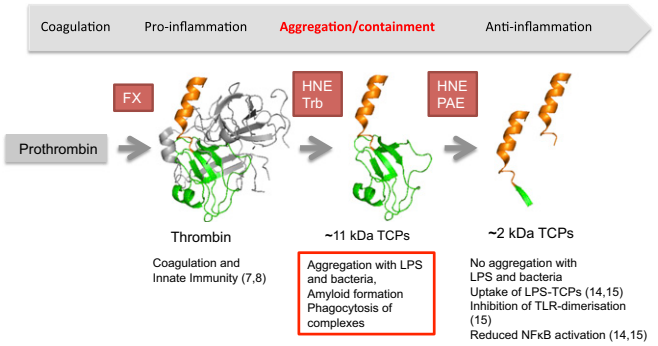

Fig. 5. Multiple effects of thrombin and its fragments. Injury and infection activate the coagulation cascade resulting in Factor X (FX)-mediated cleavage of prothrombin. Thrombin is further cleaved by HNE, generating TCPs, or autoproteolysed (Trb) (39). Further proteolysis by endogenous HNE or bacterial elastases such as lasB from *P. aeruginosa* (PAE) gives rise to short TCPs (references in parentheses). The red-colored frame indicates the findings presented in this work.

concentrations of imidazole (200 mM). The $rTCP_{96}$ was desalted in 10 mM Tris (pH 7.4) by stepwise dialysis, concentrated using a 3-kDa molecular mass cutoff Amicon ultracentrifugal filter device (Millipore), and stored at 4 °C before use (35). Peptide purity was confirmed via tricine gel electrophoresis, followed by Gel Code Blue Safe Protein staining (Thermo Scientific) and Western blotting, as noted above. The protein concentration was determined by a Nanodrop spectrometer (ND 1000; Thermo Scientific).

Heparin-Affinity Chromatography. We subjected $rTCP_{96}$ and γ-thrombin (10–30 μg) to fast protein liquid chromatography (ÄKTA purifier; GE Healthcare) using a HiTrap 1-mL heparin HP column (GE Healthcare). After injection, the samples were eluted with a linear gradient of 0–1 M NaCl in 10 mM Tris (pH 7.4).

Extraction of Thrombin Fragments from Fibrin Sloughs and a Wound Dressing. The fibrin sloughs were freeze-dried using the freeze-drying system Freezone Plus 6 (Labconco). The freeze-dried samples of the fibrin sloughs (≈7 mg) and 1 cm^2 of wound dressing (Allevyn) were incubated with 300 μL of SDS loading buffer and homogenized using a MagNA Lyser homogenizer (Roche). The homogenized samples were boiled for 10 min at 95 °C. We analyzed the protein/peptide composition of the extracts via electrophoresis and then Western blotting, as noted above.

VCA. To determine the antibacterial activity of $rTCP_{96}$, we used *E. coli* ATCC 25922. The bacteria were grown to midlogarithmic phase in 10 mL of Todd–Hewitt (TH) medium. The bacteria were centrifuged, washed, and suspended in 10 mL of 10 mM Tris buffer (pH 7.4). Next, *E. coli* ATCC 25922 (50 μL, 2×10^6 cfu/mL) was incubated with 3–6 μM $rTCP_{96}$, GKY25, or buffer control [10 mM Tris buffer (pH 7.4)] for 2 h at 37 °C. Dilution series of the incubated samples were plated on TH medium agar plates and incubated overnight at 37 °C, and we then calculated the number of colony-forming units.

RDA. We used *E. coli* ATCC 25922 and *P. aeruginosa* ATCC 27852 for the RDAs. The bacteria were grown to midlog phase in 10 mL of TH medium, spun down, washed, and suspended in 10 mL of 10 mM Tris buffer (pH 7.4). This step was followed by the addition of bacteria (4×10^6) to 15 mL of underlay agarose gel, consisting of 0.03% TH medium, 1% (wt/vol) low-electroendosmosis-type (EEO) agarose (Sigma–Aldrich), and 0.02% (vol/vol) Tween 20 (Sigma–Aldrich). The underlay was poured into a 144-mm-diameter Petri dish. After solidification, 4-mm-diameter wells were punched in the underlay, which were subsequently loaded with 6 μL of 10 μM GKY25 or $rTCP_{96}$ in 10 mM Tris buffer (pH 7.4). The plates were thereafter incubated for 3 h at 37 °C. Molten overlay gel (15 mL, 6% TH medium and 1% low-EEO agarose in water) was added to the plate. We measured the antimicrobial activity of the peptides by measuring the radius of the clearing zone surrounding the wells after 18–24 h of incubation at 37 °C.

Gel-Overlay Assay. A gel-overlay assay was performed on duplicate samples that were run on a nondenaturing acid urea (AU) PAGE gel in 5% acetic acid at 100 V for 75 min using reversed polarity. Bacterial precultures were grown overnight in 10 mL of TH broth, inoculated the subsequent day, and grown until their optical density reached 0.4. The bacteria were washed, and the pellet was resuspended in 10 mM Tris (pH 7.4). The bacteria (4×10^6) were added to 15 mL of melted underlay agarose [10 mM Tris (pH 7.4), 0.03% TH broth, 1% agarose type, 1% low-EEO agarose] and poured into Petri dishes. One AU gel was stained with Coomassie Brilliant Blue, and the other was washed three times with 10 mM Tris (pH 7.4) for 4 min and then placed on the top of the underlay gel, followed by incubation for 3 h at 37 °C. Overlay agar (15 mL) was poured over the underlay and left to solidify. The inhibition zones were measured using electronic digital calipers (Perel) after 16 h of incubation at 37 °C.

Slot-Blot Assay. We used a slot-blot assay to detect the interaction between $rTCP_{96}$ and LPS. The $rTCP_{96}$ and GKY25 (2 μg and/or 5 μg per well) were bound to nitrocellulose membrane (Hybond-C; GE Healthcare Biosciences) after presoaking in 10 mM Tris (pH 7.4). The membrane was incubated in the blocking solution [2% BSA in PBS (pH 7.4)] for 1 h at room temperature and subsequently incubated with 20 μg/mL biotinylated LPS (LPS-EB Biotin; InvivoGen) in PBS for 1 h at room temperature. Next, the membranes were washed three times for 10 min in PBS and incubated with streptavidin-HRP conjugate (Thermo Scientific). Binding was detected using peroxide solution and a luminol/enhancer solution (1:1 vol/vol, SuperSignal West Pico Chemiluminescent Substrate; Thermo Scientific). To test for competitive inhibition of peptide binding to LPS, we also performed binding studies in the presence of unlabeled heparin (6 mg/mL).

Fluorescence Microscopy. FITC is a fluorescent probe able to permeate the membranes of dead bacteria and to bind to bacterial DNA, which is detected as a green fluorescent signal. *E. coli* ATCC 25922 was grown to midlogarithmic phase in 10 mL of TH medium. The bacteria were centrifuged, washed, and suspended in 10 mL of 10 mM Tris (pH 7.4). Next, *E. coli* ATCC 25922 (100 μL, 1×10^7 cfu/mL) was incubated with 10 μM GKY25, $rTCP_{96}$, or control [10 mM Tris (pH 7.4)] for 1 h at 37 °C. The microorganisms were incubated on poly (L-lysine)–coated glass slides via incubation for 45 min at 37 °C. Next, 200 μL of FITC (6 μg/mL) was added to the top of each slide. The samples were thereafter fixed with 2% paraformaldehyde for 15 min at 4 °C and for 45 min at room temperature. The cover slides were mounted on microscope slides with fluorescent mounting media (Dako). A Nikon Eclipse TE300 inverted fluorescent microscope (Nikon) supplied with a Hamamatsu C4742-95 cooled CCD camera (Hamamatsu) and a Plan Apochromat 100× objective (Olympus) was used to acquire images of the FITC-stained bacteria. We used the imaging software NIS-elements 3.1 (Nikon) for the image acquisition and processing.

ThT Dye-Binding Assays. Amyloid formation was determined using the dye ThT. ThT preferentially binds to the β-sheet structures of amyloidogenic proteins/peptides. For the assay, $rTCP_{96}$ (10 μM), GKY25 (10 μM), α-thrombin (10 μM ± HNE), γ-thrombin (10 μM), LPS (100 μg/mL), or buffer only [10 mM Tris (pH 7.4)] was incubated with LPS for 30 min at 37 °C. For examination of the time dependence of the aggregation, $rTCP_{96}$ (10 μM) was incubated for 10, 30, 60, and 120 min at 37 °C in the absence or presence of LPS in 10 mM Tris (pH 7.4). For examination of the concentration dependence of the aggregation, $rTCP_{96}$ (0.1, 0.5, 1, 2, 5, and 10 μM) was incubated for 30 min at 37 °C in the absence or presence of LPS in 10 mM Tris (pH 7.4). In one experiment, the buffer was supplemented with 1% citrated plasma. For evaluation of the effects of GKY25 on the aggregation, GKY25 (1, 5, 10, and 20 μM) was added to $rTCP_{96}$ (10 μM) and LPS (100 μg/mL) in 10 mM Tris (pH 7.4), followed by a 30-min incubation period. Two hundred microliters of the materials was incubated with ThT (final concentration of 10 μM) for 15 min in the dark [1 mM ThT stock was stored in the dark at 4 °C in 0.1 M glycine (pH 8.5)]. We measured ThT fluorescence using a VICTOR3 Multilabel Plate Counter spectrofluorometer (PerkinElmer) at an excitation of 450 nm, with excitation and emission slit widths of 10 nm. The baseline (10 mM Tris buffer, LPS or HNE) was subtracted from the signal of each sample (18).

CD. We performed CD measurements on a Jasco J-810 spectropolarimeter equipped with a Jasco CDF-426S Peltier set to 25 °C. The peptides/proteins were diluted to 10 μM in Tris buffer (10 mM, pH 7.4) and incubated with 10 μM LPS for 1 h at 37 °C; placed in a 10-mm quartz cuvette; and, after extensive purging with nitrogen, scanned over the wavelength interval 200–260 nm (scan speed of 20 $nm \cdot min^{-1}$). We calculated the averages of five scans for each sample. For examination of time dependence, $rTCP_{96}$ (10 μM) was incubated for 10 and 120 min at 37 °C in absence or presence of LPS (100 μg/mL) in 10 mM Tris (pH 7.4). The baseline (10 mM Tris buffer, LPS or HNE) was subtracted from the spectra of each sample.

TEM. We visualized the aggregates formed by $rTCP_{96}$ in plasma alone, or in the presence of LPS or *E. coli*, of HNE-treated α-thrombin (10 μM) or

γ-thrombin alone (10 μM) after incubation with LPS using TEM (Jeol Jem 1230) in combination with negative staining. The samples were adsorbed onto carbon-coated grids for 60 s and stained with 7 μL of 2% uranyl acetate for 20 s. The grids were rendered hydrophilic via glow discharge at low pressure in air.

Furthermore, we used TEM to study the aggregation of endogenous thrombin fragments in acute wound fluids. Polyclonal rabbit antibodies (against the VFR17 epitope) were labeled with gold particles 20 nm in diameter; they were subsequently added to acute wound fluids and incubated for 30 min at 37 °C. We also performed TEM analysis of TCPs and LPS in fibrin sloughs by incubating the material with gold-labeled VFR17 antibodies, followed by incubation with gold-labeled anti-rabbit IgG (10 nm). Electron micrographs of the fibril sloughs were captured using a Philips/FEI CM100 electron microscope. The detection of LPS was performed using IgG against LPS with labeled gold particles 5 nm in diameter. Analysis of the distribution and possible colocalization of large and small gold particles, representing TCPs and LPS, respectively, was performed using the plug-in "Gold" in the Ellipse program (nucleus.img.cas.cz/gold/) (24).

Phagocytosis Assay. The macrophage cell line RAW 264.7 (passages 8–10), grown in DMEM with 10% (vol/vol) FBSi and 1% (vol/vol) AA, was seeded in 96-well tissue culture plates (8×10^4 cells per well) overnight at 37 °C in a 5% CO_2 atmosphere. pHrodo Green *E. coli* BioParticles (Life Technologies) were resuspended in 2 mL of Hanks' balanced salt solution (Life Technologies) and pretreated with 1.0 and 0.5 μM $rTCP_{96}$ in 10 mM Tris for 1 h at 37 °C. The pretreated suspension of *E. coli* BioParticles was added to the adherent RAW 264.7 cells. To analyze phagocytosis, the particles were incubated with the cells for 1.5 h at 37 °C. We then measured fluorescence using a VICTOR3 Multilabel Plate Counter spectrofluorometer (PerkinElmer) at excitation/emission wavelengths of 485/535 nm. The baseline uptake (of only *E. coli* BioParticles) was subtracted from the signal of each sample.

Confocal Microscopy. We performed ThT staining to visualize amyloid formation of 10 μM $rTCP_{96}$ and endogenous TCPs in selected acute wound fluids, which were induced by LPS and/or *E. coli* ATCC 25922. The bacterial suspension was prepared as described above for RDAs and VCAs. The LPS/*E. coli*-treated samples of acute wound fluids/$rTCP_{96}$ were fixed and washed as described above (FITC staining). The samples were subsequently incubated with 200 μL of ThT (25 μM) on slides for 30 min at 37 °C. The primary antibodies against the TCP sequence were added to the samples containing wound fluid, followed by the washing step and the addition of secondary antibodies. The incubation parameters were adopted from the Western blotting technique (discussed above), and the incubation duration of each antibody was 30 min at 37 °C. The cover slides (Thermo Scientific) were mounted on microscope slides with fluorescent mounting media (Molecular Probes; Life Technologies).

RAW 264.7 cells (200,000 cells per milliliter) were seeded on round cover glasses and incubated overnight to enable adherence. The next day, the *E. coli* particles were preincubated with 1 μM TCP as described in the phagocytosis assay. Fixed cells were permeabilized with 0.5% Triton diluted in PBS for 2 min at room temperature. The staining method to visualize TCP was performed as described above. The samples were mounted with ProLong Gold with DAPI (Life Technologies) to stain the nuclei.

We examined the mounted samples using an LSM 700 laser-scanning confocal microscope (Zeiss) with excitation wavelengths of 488 nm and 568 nm and a C-Apochromat 63×/1.20-W Korr M27 glycerol immersion objective. Images were collected using Zen 2012 software and analyzed using ImageJ software (version 1.49q; NIH).

Hemolysis Assay. Fresh citrated venous blood from healthy donors (two female and one male) was centrifuged at 250 × *g*, and the pellet was washed three times with PBS. Next, the pellet was diluted five times, and 5 μL of this solution was transferred to each well of a 96-well plate containing 195 μL of $rTCP_{96}$ (0.1, 1, 2, 5, and 10 μM) in PBS. After 1 h of incubation at 37 °C and 5% CO_2, the plate was centrifuged at 800 × *g*. Next, 150 μL of each sample was transferred to a flat-bottomed 96-well plate, and the absorbance at 450 nm was measured. The results are expressed as a percentage of the erythrocyte lysis compared with the positive control (2.5% Tween-20). Values below 10% are regarded as nonhemolytic.

Ellipsometry. Peptide adsorption was studied in situ by null ellipsometry (36) using an Optrel Multiskop (Optrel) equipped with a 100-mW Nd:YAG laser (JDS Uniphase). All of the measurements were carried out at 532 nm, and at an angle of incidence of 67.66° in a 5-mL cuvette under stirring (300 rpm) using regulator rotor Mascot 8610 (Elfa). The principles of null ellipsometry and the procedures used have both been described previously in the literature (37). In brief, by monitoring the change in the state of polarization of light reflected at a surface in the absence and presence of an adsorbed layer, the mean refractive index (n) and layer thickness (d) of the adsorbed layer can be obtained. Based on the thickness and the refractive index, we calculated the adsorbed amount (Γ) using the following equation (36):

$$\Gamma = \frac{(n - n_0)}{dn/dc} d,$$

where dn/dc (0.154 cm^3/g) is the refractive index increment and n_0 is the refractive index of the bulk solution. Corrections were routinely applied to the bulk refractive index to account for changes in temperature and excess electrolyte concentration.

LPS-coated surfaces were obtained by adsorbing *E. coli* LPS to methylated silica surfaces [surface potential of −40 mV and contact angle of 90° (38)] from 5 mg/mL LPS stock solution in water at a concentration of 0.4 mg/mL in 10 mM Tris (pH 7.4). This LPS concentration corresponds to saturation in the LPS adsorption isotherm (1.48 ± 0.38 mg/m^2) under these conditions. Nonadsorbed LPS was removed by rinsing with Tris buffer at 5 $mL \cdot min^{-1}$ for a period of 30 min and allowing the buffer to stabilize for 20 min. Peptide addition was subsequently performed to 0.01, 0.1, 0.5, and 1 μM, and adsorption was monitored for at least 1 h after each addition. All of the measurements were performed in at least triplicate at 25 °C.

Molecular Dynamics Simulations. The crystal structure of human γ-thrombin was retrieved from the Protein Data Bank (39). The 11-kDa TCP was modeled using a single chain of the γ-thrombin structure. The extracted chain was placed in a cubic box of TIP3P water molecules at a salt concentration of 0.1 M (40). An atomistic model of the 11-kDa TCP was derived using the Amber force field ff14SB (41). The 11-kDa TCP was simulated for 100 ns in the NpT ensemble at 300 K and 1 bar to assess the stability of the fold. In parallel, a CG model of TCP was derived from the same starting structure using the MARTINI force field (42). The CG model was incubated with a single lipid A molecule and simulated for 5 × 1 μs to determine the preferential interaction sites of TCP with LPS. Preferential sites comprise the newly exposed residues 44–62 and 80–96 for the lipid tails of LPS and residues 1–20 for the polar head of LPS. Next, the TCP molecules were incubated with and without eight LPS molecules to study aggregation behavior. We performed 5 × 1-μs simulations for both the eight TCPs system and the eight TCPs with eight LPSs system. We calculated the pairwise distances between all of the residues on the TCP molecules and summed them over all of the intermolecular interactions. The resulting average distances reveal increased aggregation at sites that had previously been identified to interact preferentially with LPS.

In Silico Modeling of TCP Fold Stability and Secondary Structure. The region corresponding to amino acids 527–622 (prothrombin numbering) was extracted from the structure of full-length thrombin. It was simulated in explicit TIP3P water molecules at a salt concentration of 0.1 M for 1 μs using the Amber force field ff14SB (41), and exhibited a stable fold. After initial reorganization of the N- and C-terminal segments, the core of the rTCP retains its original structure. Quantitatively, the rmsd between the simulated rTCP and the TCP fragment within the gamma-thrombin X-ray structure is 0.25 nm. Mean secondary structural contents during the equilibrated simulation period were calculated using STRIDE (https://doi.org/10.1093/nar/gkh429) as implemented in VMD 1.9.2 (PubMed identifier: 8744570).

MST. We performed MST analysis using a NanoTemper Monolith NT.115 apparatus (NanoTemper Technologies). We used a Monolith NT Protein Labeling Kit RED–NHS (NanoTemper Technologies) to label 10 μM $rTCP_{96}$ according to the manufacturer's protocol. A constant amount of 1.5 μM $rTCP_{96}$ was mixed with increasing concentrations of LPS in Tris buffer (10 mM, pH 7.4). Next, 10 μL of the samples was loaded into standard glass capillaries (Monolith NT Capillaries; NanoTemper Technologies), and we performed the MST analysis (settings for the light-emitting diode and infrared laser were 80%). Labeled IVE25 was added to LPS under the same conditions as above and used as a negative control.

DLS. We performed DLS measurements to measure the hydrodynamic radii of $rTCP_{96}$, LPS, and LPS-$rTCP_{96}$. Wyatt quasi-elastic light scattering (Wyatt Technology Corporation) and a Dawn enhanced optical system (Wyatt Technology Corporation) equipped with a temperature-controlled microsampler instrument were used for DLS measurements. We incubated the samples for 1 h at 37 °C under reducing conditions, and the scattered light was detected at 18 different angles simultaneously. Before the experiment,

all samples were filtered through 0.22-μm pore-sized microfilters (Sartorius). Aliquots of samples were manually loaded into the flow cell and measured at 37 °C. All samples (1 μM $rTCP_{96}$, 1 μM LPS, and 1 μM LPS-$rTCP_{96}$, respectively) were measured at least 15 times. GKY25 peptide was used as a negative control and analyzed under the same conditions. For evaluation of the time dependence of the aggregation, $rTCP_{96}$ (1 μM) was incubated for 10, 30, 60, and 120 min at 37 °C in the absence or presence of LPS (10 μg/mL) in 10 mM Tris (pH 7.4). The hydrodynamic radii were analyzed by Astra V software using Zimm modeling.

Statistical Analysis. The diagrams of the RDA, VCA, ThT assay, DLS assay, and hemolysis assay are presented as means and SDs from at least three independent experiments. We assessed differences in these assays using one-way ANOVA with Dunnett's multiple comparison tests and two-way ANOVA with Sidak's multiple comparison tests. All of the data were analyzed using GraphPad Prism (GraphPad Software, Inc.). A P value less than 0.05 was considered to be statistically significant (*$P < 0.05$, **$P < 0.01$, ***$P < 0.001$, and ****$P < 0.0001$).

ACKNOWLEDGMENTS. We thank Maria Baumgarten and Lisa-Britt Wahlberg for excellent technical assistance with the TEM preparation and ellipsometry, respectively. We acknowledge the Lund University Bioimaging Center for access to EM facilities. We are indebted to Dr. Sven Kjellström (Department of Biochemistry and Structural Biology, Center for Molecular and Protein Science, Lund University) for verification of the amino acid sequence of $rTCP_{96}$ via electrospray ionization mass spectrometry. We acknowledge Dr. Vlada Philimonenko [Microscopy Center, Electron Microscopy Core Facility, Institute of Molecular Genetics of the Academy of Sciences of the Czech Republic, supported by the Ministry of Education, Youth and Sports of the Czech Republic (LM2015062 Czech-BioImaging)] for statistical analysis of colocalization on the immunogold-labeled electron microscopy samples. This work was supported by grants from the Swedish Research Council (Projects 2012-1883 and 2012-1842); the O. E. and Edla Johanssons, Welander–Finsen, Crafoord, Österlund, Söderberg, and Knut and Alice Wallenberg Foundations; the Swedish Foundation for Strategic Research; The Swedish Government Funds for Clinical Research; and the medical faculty of Lund University.

1. Tennessen JA (2005) Molecular evolution of animal antimicrobial peptides: Widespread moderate positive selection. *J Evol Biol* 18:1387–1394.
2. Zanetti M (2004) Cathelicidins, multifunctional peptides of the innate immunity. *J Leukoc Biol* 75:39–48.
3. Zasloff M (2002) Antimicrobial peptides of multicellular organisms. *Nature* 415: 389–395.
4. Huttner KM, Bevins CL (1999) Antimicrobial peptides as mediators of epithelial host defense. *Pediatr Res* 45:785–794.
5. Kalle M, et al. (2013) Proteolytic activation transforms heparin cofactor II into a host defense molecule. *J Immunol* 190:6303–6310.
6. Papareddy P, et al. (2014) Antimicrobial effects of helix D-derived peptides of human antithrombin III. *J Biol Chem* 289:29790–29800.
7. Bode W (2006) The structure of thrombin: A janus-headed proteinase. *Semin Thromb Hemost* 32:16–31.
8. Davie EW, Kulman JD (2006) An overview of the structure and function of thrombin. *Semin Thromb Hemost* 32:3–15.
9. Brower MS, Walz DA, Garry KE, Fenton JW, 2nd (1987) Human neutrophil elastase alters human alpha-thrombin function: Limited proteolysis near the gamma-cleavage site results in decreased fibrinogen clotting and platelet-stimulatory activity. *Blood* 69:813–819.
10. Papareddy P, et al. (2010) Proteolysis of human thrombin generates novel host defense peptides. *PLoS Pathog* 6:e1000857.
11. Angus DC, van der Poll T (2013) Severe sepsis and septic shock. *N Engl J Med* 369:2063.
12. Kalle M, et al. (2012) Host defense peptides of thrombin modulate inflammation and coagulation in endotoxin-mediated shock and Pseudomonas aeruginosa sepsis. *PLoS One* 7:e51313.
13. Papareddy P, et al. (2010) C-terminal peptides of tissue factor pathway inhibitor are novel host defense molecules. *J Biol Chem* 285:28387–28398.
14. van der Plas MJ, et al. (2016) Pseudomonas aeruginosa elastase cleaves a C-terminal peptide from human thrombin that inhibits host inflammatory responses. *Nat Commun* 7:11567.
15. Hansen FC, et al. (2015) The thrombin-derived host defense peptide GKY25 inhibits endotoxin-induced responses through interactions with lipopolysaccharide and macrophages/monocytes. *J Immunol* 194:5397–5406.
16. Carter WJ, Cama E, Huntington JA (2005) Crystal structure of thrombin bound to heparin. *J Biol Chem* 280:2745–2749.
17. Singh S, Kalle M, Papareddy P, Schmidtchen A, Malmsten M (2013) Lipopolysaccharide interactions of C-terminal peptides from human thrombin. *Biomacromolecules* 14: 1482–1492.
18. Petrlova J, et al. (2014) Conformational and aggregation properties of the 1-93 fragment of apolipoprotein A-I. *Protein Sci* 23:1559–1571.
19. Biancalana M, Koide S (2010) Molecular mechanism of Thioflavin-T binding to amyloid fibrils. *Biochim Biophys Acta* 1804:1405–1412.
20. Fenton JW, Landis BH, Walz DA, Finlayson JS (1977) *Human Thrombin* (Ann Arbor Science Publishers, Ann Arbor, MI).
21. Liu CY, Nossel HL, Kaplan KL (1979) The binding of thrombin by fibrin. *J Biol Chem* 254:10421–10425.
22. Lundqvist K, Herwald H, Sonesson A, Schmidtchen A (2004) Heparin binding protein is increased in chronic leg ulcer fluid and released from granulocytes by secreted products of Pseudomonas aeruginosa. *Thromb Haemost* 92:281–287.
23. Schmidtchen A (2000) Degradation of antiproteinases, complement and fibronectin in chronic leg ulcers. *Acta Derm Venereol* 80:179–184.
24. Philimonenko AA, Janácek J, Hozák P (2000) Statistical evaluation of colocalization patterns in immunogold labeling experiments. *J Struct Biol* 132:201–210.
25. Landreh M, Johansson J, Jörnvall H (2014) Separate molecular determinants in amyloidogenic and antimicrobial peptides. *J Mol Biol* 426:2159–2166.
26. Scott MG, Davidson DJ, Gold MR, Bowdish D, Hancock REW (2002) The human antimicrobial peptide LL-37 is a multifunctional modulator of innate immune responses. *J Immunol* 169:3883–3891.
27. Soscia SJ, et al. (2010) The Alzheimer's disease-associated amyloid beta-protein is an antimicrobial peptide. *PLoS One* 5:e9505.
28. Spitzer P, et al. (2016) Amyloidogenic amyloid-β-peptide variants induce microbial agglutination and exert antimicrobial activity. *Sci Rep* 6:32228.
29. Papareddy P, Mörgelin M, Walse B, Schmidtchen A, Malmsten M (2012) Antimicrobial activity of peptides derived from human ß-amyloid precursor protein. *J Pept Sci* 18: 183–191.
30. Pasupuleti M, et al. (2009) Antimicrobial activity of human prion protein is mediated by its N-terminal region. *PLoS One* 4:e7358.
31. Zenaro E, et al. (2015) Neutrophils promote Alzheimer's disease-like pathology and cognitive decline via LFA-1 integrin. *Nat Med* 21:880–886.
32. Deng X, et al. (2014) Lipolysaccharide-induced neuroinflammation is associated with Alzheimer-like amyloidogenic axonal pathology and dendritic degeneration in rats. *Adv Alzheimer Dis* 3:78–93.
33. Grammas P, Martinez JM (2014) Targeting thrombin: An inflammatory neurotoxin in Alzheimer's disease. *J Alzheimers Dis* 42:S537–S544.
34. Taylor SC, Berkelman T, Yadav G, Hammond M (2013) A defined methodology for reliable quantification of Western blot data. *Mol Biotechnol* 55:217–226.
35. Petrlova J, et al. (2011) A differential association of Apolipoprotein E isoforms with the amyloid-β oligomer in solution. *Proteins* 79:402–416.
36. Azzam RMA, Bashara NM (1977) *Ellipsometry and Polarized Light* (Elsevier North-Holland, Amsterdam).
37. Malmsten M (1994) Ellipsometry studies of protein layers adsorbed at hydrophobic surfaces. *J Colloid Interface Sci* 166:333–342.
38. Malmsten M, Burns N, Veide A (1998) Electrostatic and hydrophobic effects of oligopeptide insertions on protein adsorption. *J Colloid Interface Sci* 204:104–111.
39. Rydel TJ, et al. (1994) Crystallographic structure of human gamma-thrombin. *J Biol Chem* 269:22000–22006.
40. Jorgensen WL, Chandrasekhar J, Madura JD, Impey RW, Klein ML (1983) Comparison of simple potential functions for simulating liquid water. *J Chem Phys* 79:926–935.
41. Maier JA, et al. (2015) ff14SB: Improving the accuracy of protein side chain and backbone parameters from ff99SB. *J Chem Theory Comput* 11:3696–3713.
42. Monticelli L, et al. (2008) The MARTINI coarse-grained force field: Extension to proteins. *J Chem Theory Comput* 4:819–834.